

# Amorphous Formulations of Indomethacin and Griseofulvin Prepared by Electrospinning

Felipe L. Lopez,<sup>†</sup> Gemma C. Shearman,<sup>‡</sup> Simon Gaisford,<sup>\*,†</sup> and Gareth R. Williams<sup>\*,†</sup>

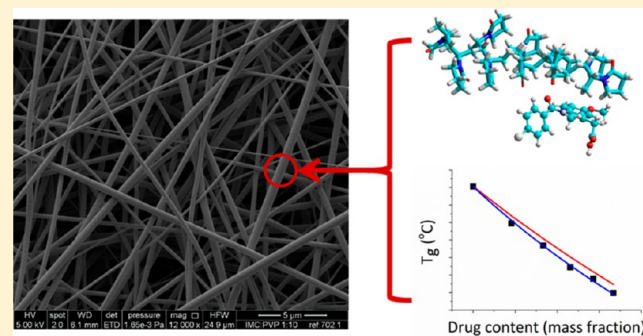
<sup>†</sup>UCL School of Pharmacy, University College London, 29–39 Brunswick Square, London WC1N 1AX, United Kingdom

<sup>‡</sup>School of Human Sciences, London Metropolitan University, 166–220 Holloway Road, London N7 8DB, United Kingdom

## Supporting Information

**ABSTRACT:** Following an array of optimization experiments, two series of electrospun polyvinylpyrrolidone (PVP) fibers were prepared. One set of fibers contained various loadings of indomethacin, known to form stable glasses, and the other griseofulvin (a poor glass former). Drug loadings of up to 33% w/w were achieved. Electron microscopy data showed the fibers largely to comprise smooth and uniform cylinders, with evidence for solvent droplets in some samples. In all cases, the drug was found to exist in the amorphous physical state in the fibers on the basis of X-ray diffraction and differential scanning calorimetry (DSC) measurements. Modulated temperature DSC showed that the relationship between a formulation's glass transition temperature ( $T_g$ ) and the drug loading follows the Gordon–Taylor equation, but not the Fox equation. The results of Gordon–Taylor analysis indicated that the drug/polymer interactions were stronger with indomethacin. The interactions between drug and polymer were explored in more detail using molecular modeling simulations and again found to be stronger with indomethacin; the presence of significant intermolecular forces was further confirmed using IR spectroscopy. The amorphous form of both drugs was found to be stable after storage of the fibers for 8 months in a desiccator (relative humidity <25%). Finally, the functional performance of the fibers was studied; in all cases, the drug-loaded fibers released their drug cargo very rapidly, offering accelerated dissolution over the pure drug.

**KEYWORDS:** *electrospinning, nanofiber, amorphous, indomethacin, griseofulvin, modulated-temperature DSC*



## INTRODUCTION

The amorphous form is of major interest to pharmaceutical scientists because of the enhancement in dissolution rate and bioavailability it can offer over crystalline materials. However, amorphous materials are always metastable, and will over time relax to a crystalline state. Understanding and quantifying the rate and extent of this transformation is key to the development of robust medicines which perform consistently.<sup>1</sup>

The electrospinning approach has been widely applied to the production of amorphous formulations of active pharmaceutical ingredients (APIs). The technique uses electrical energy to evaporate solvent from a solution to generate a solid product. It is attractive in its simplicity and low cost. In a typical experimental setup, a syringe is filled with a solution of a polymer and drug in a volatile solvent. A metal dispensing tip (spinneret) is attached to the syringe, and a pump used to expel liquid at a controlled rate. A high (kV) voltage is applied between the spinneret and a metal collector (commonly a flat plate coated in Al foil). The electrical energy causes the droplets ejected from the syringe to elongate to form a Taylor cone, which subsequently emits straight jets of fluid. This ultimately leads to evaporation of the solvent, and the formation of a solid product in the form of one-dimensional polymer fibers with a drug embedded. Importantly, this process

is usually very rapid, occurring on the order of  $10^{-2}$  s in many cases.<sup>2,3</sup> This leads to the physical state of the components in the liquid phase being propagated into the solid state: as a result, solid solutions of a drug in polymer are often produced because the drug molecules have no time to undergo crystallization.

There are myriad examples of electropun polymer fibers being used to render drugs amorphous: for instance, Illangakoon et al. have recently created amorphous formulations of mebeverine hydrochloride in polyvinylpyrrolidone (PVP) and Eudragit-based fibers.<sup>4</sup> Verreck in an early study in 2003 demonstrated that the poorly soluble itraconazole could be rendered amorphous in electrospun hydroxypropyl methylcellulose fibers,<sup>5</sup> and Yu et al. have demonstrated analogous results using ibuprofen and PVP.<sup>6</sup> Electrospun materials have been widely explored in pharmaceutical applications, for instance, to deliver antibiotics.<sup>7,8</sup> The interested reader is directed to a recent review for a more detailed survey of such systems.<sup>9</sup> Although much work has been undertaken to look at

Received: May 30, 2014

Revised: September 4, 2014

Accepted: October 15, 2014

Published: October 15, 2014



whether the electrospinning route may be used to enhance the solubility of poorly soluble APIs, and the role of drug solubility in the polymer carrier has also been probed,<sup>10</sup> as far as the authors are aware there are no studies where the influence of the API's glass-forming ability is investigated. Therefore, in this paper, the electrospinning of polymer fibers containing two drugs with very different glass-forming properties was explored. The drugs selected for study were indomethacin ( $T_g/T_m = 0.73$ ), which forms very stable glasses,<sup>11</sup> and griseofulvin ( $T_g/T_m = 0.74$ ), the amorphous form of which relaxes to become crystalline very rapidly.<sup>12</sup> The chemical structure of these APIs is given in Figure 1.

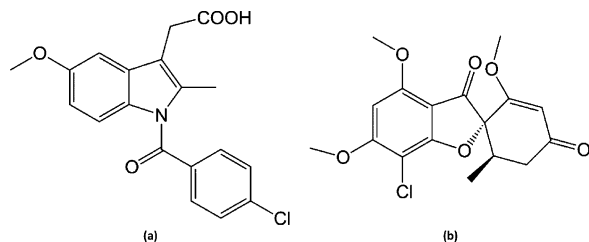


**Figure 1.** Chemical structures of (a) indomethacin and (b) griseofulvin.

Griseofulvin is an antifungal agent commonly used to treat skin conditions, whereas indomethacin is a nonsteroidal anti-inflammatory drug indicated for the relief of pain and stiffness. Both are given as oral formulations, and for both APIs, amorphous formulations could be useful for the rapid treatment of symptoms. In addition, both have rather bitter tastes, and their incorporation into a system where taste masking can be achieved is thus a useful aim. Preparing electrospun fibers of the APIs offers the potential to create oral fast-dissolving films that may be administered for instance in a sublingual or buccal manner.<sup>6,13,14</sup>

A comprehensive search of the literature revealed no examples of electrospun griseofulvin systems. In contrast, a number of authors have previously produced electrospun indomethacin (IMC) formulations. For instance, Taepaiboon et al. prepared fibers with IMC embedded in poly(vinyl alcohol) (PVA), with up to 16.7% w/w drug loaded in the polymer.<sup>15</sup> These authors observed some "bead-on-string" morphology in their fibers, in which the drug was found to be in a crystalline state. The fibers were not found to enhance the dissolution rate of IMC compared to equivalent IMC/PVA casting films. In other work, Pornsopone and co-workers<sup>16</sup> spun IMC-containing fibers using some methacrylate polymers but did not comment on the physical form of the drug in the formulation. Tungprapa et al. generated IMC-loaded cellulose acetate fibers (drug loading: 16.7% w/w) and observed that the fibers released IMC more rapidly than the analogous casting films.<sup>17</sup> Trout's team prepared IMC-containing polyvinylpyrrolidone (PVP) fibers, in which the drug was observed to be amorphous and to remain without crystalline character after 6 months' storage at 40 °C.<sup>18</sup> These authors also found it was possible to prepare PVP/IMC fibers with very high drug loadings (up to 50% w/w), with the drug being amorphous even at the highest loadings.<sup>19</sup> No functional performance studies were undertaken, however, and so it is not known how these fibers might affect the drug release rate and extent. In other work, Rasekh and co-workers have very recently deposited electrospun PVP/IMC fibers onto plasters for

wound healing applications.<sup>20</sup> Multicomponent systems containing IMC, a polymer, and Fe<sub>3</sub>O<sub>4</sub> nanoparticles have also recently been prepared and explored with regard to achieving controlled and targeted drug release under the influence of an external magnetic field.<sup>21</sup>

In this work, we selected the FDA-approved generally regarded as safe (GRAS) polymer polyvinylpyrrolidone (PVP) and explored the influence of an API's glass forming ability on the PVP-API fibers produced by electrospinning. A side-by-side study was undertaken in which equivalent indomethacin and griseofulvin fibers were prepared. The influence of a range of spinning parameters on fiber formation was explored, and the optimized set of fibers fully characterized in terms of their physicochemical properties, storage stability, and functional performance.

## EXPERIMENTAL SECTION

**Materials.** Indomethacin (IMC) was supplied by the Wuhan Yuancheng Gongchuan Technology Co. (Hubei, China) and griseofulvin (GSF) by Molekula Ltd. (Gillingham, U.K.). Polyvinylpyrrolidone K60 (PVP; molecular weight ca. 360 000), was purchased from Sigma-Aldrich (Gillingham, U.K.). N,N-dimethylacetamide (DMAc) was procured from Sigma-Aldrich, and acetone (HPLC Chromasolv grade) and methanol (AR grade) were sourced from Fisher Scientific Ltd. (Loughborough, U.K.). Phosphate buffered saline (PBS, pH = 7.4) powder was obtained from Sigma-Aldrich.

**Electrospinning.** Solutions for electrospinning (ES) were prepared by dissolving the required amounts of drug and polymer in ethanol/DMAc (2:1 v/v), or acetone/DMAc (2:1 v/v). The API was added to 10 mL of solvent in a clear glass vial and stirred at room temperature (RT) for ca. 1 h until complete dissolution was achieved. Thereafter, 1000 mg of PVP was slowly added and the codissolving solutions stirred overnight at RT. During stirring, glass vials were sealed with a rubber cap to avoid solvent evaporation. Full details of the solutions prepared are given in later sections of this manuscript.

For ES, the API/polymer solution was loaded into a 5 mL plastic syringe to which a stainless steel needle (spinneret) was attached. A high voltage DC power supply (HCP 35–35 000, FuG Elektronik, Rosenheim, Germany) was employed to provide a high voltage between the spinneret (connected to the positive electrode) and a metal collector plate (connected to the grounded electrode). The collector was wrapped in aluminum foil and set at a constant distance from the tip of the spinneret. Experiments were performed with two different spinners (internal diameter [I.D.] 0.84 or 0.33 mm). For all experiments, the applied voltage was 12 kV, and the spinneret-to-collector distance 15 cm. All processes were conducted at ambient temperature and pressure. Temperature and humidity were recorded before and after manufacturing: the temperature ranged between 19 and 22 °C and the relative humidity from 20 to 35%. After manufacturing, samples were wrapped in aluminum foil and stored in a desiccator for at least 12 h prior to analysis. Silica gel was used as desiccant, maintaining the relative humidity inside the desiccator below 25%.

**Characterization. Scanning Electron Microscopy.** Scanning electron microscopy (SEM) was used to investigate the morphology of the ES formulations. Samples were cut from the fiber mats and adhered onto aluminum SEM stubs (TAAB Laboratories, Reading, U.K.) using carbon-coated double-sided tape. In order to render them conductive, they were then sputter coated with gold. Analysis was conducted using a

Quanta 200F instrument (FEI, Hillsborough, OR, U.S.A.). The average fiber diameter was determined by taking more than 50 measurements in SEM images, using the ImageJ software (National Institutes of Health, Bethesda, MD, U.S.A.).

**Differential Scanning Calorimetry.** Differential scanning calorimetry (DSC) experiments were conducted using a Q2000 DSC (TA Instruments, New Castle, DE, U.S.A.). Samples were heated from 20 to 240 °C at 10 °C min<sup>-1</sup> under a 50 mL min<sup>-1</sup> flow of N<sub>2</sub> gas. Modulated temperature DSC analysis was conducted on the same instrument from 100 to 190 °C or 90 to 240 °C using a temperature ramp of 3 °C min<sup>-1</sup> and a modulation period of 60 s. Data analysis was carried out using the TA Universal Analysis software. Amorphous samples of the pure drugs were prepared for comparison purposes by loading a DSC pan with the drug and heating it above the API's melting point (at 225 °C [GSF] and 165 °C [IMC]) for 3 min, and then cooling for 5 min on brass.

**Thermogravimetric Analysis.** Thermogravimetric analysis (TGA) was undertaken using either a TGA 2950 analyzer or a Discovery TGA instrument (both manufactured by TA Instruments). Approximately 1–3 mg of sample was placed in a Tzero aluminum pan and sealed with a pin-holed lid. After 5 min stabilization at 30 °C, the sample was heated from 30 to 190 or 240 °C at a ramp rate of 10 °C min<sup>-1</sup> under a flow of N<sub>2</sub> (50 mL min<sup>-1</sup>). Data analysis was conducted using the TA Universal Analysis software.

**X-ray Diffraction.** X-ray diffraction (XRD) patterns were acquired using a Miniflex 600 diffractometer (Rigaku, Tokyo, Japan). The instrument produces Cu K $\alpha$  radiation (1.5418 Å) at 40 kV and 15 mA, and patterns were recorded in the 2 $\theta$  range 4 to 36° at a speed of 5° min<sup>-1</sup>.

**FT-IR Spectroscopy.** Infrared spectroscopy was carried out using a Spectrum 100 FTIR spectrometer (PerkinElmer, Waltham, MA, U.S.A.) over the range 650–4000 cm<sup>-1</sup> with resolution 1 cm<sup>-1</sup>.

**Molecular Modeling.** Molecular mechanics in vacuo calculations were performed using HyperChem version 8.0.10 (a molecular modeling software package). The structures of each of the compounds were initially sketched using ChemBio Draw Ultra 12.0 or Accelrys Draw 4.1. A decameric PVP species was selected as representative of the polymer. Individual structures were then imported separately into HyperChem; for each, all hydrogen atoms were explicitly included and a 3-D trial structure based on preset bond angles and lengths was generated. The structures then underwent an initial geometric minimization with the MM+ force field followed by a full energetic minimization using the AMBER 3 (Assisted Model Building and Energy Refinement) force field. For the former, the nonbonded electrostatic interactions were calculated using bond dipole interactions whereas for the latter, the distance-dependent dielectric constant was assigned a scale factor of 1, and the 1–4 scale factors (representing the nonbonded interactions between atoms separated by three atoms) were: electrostatic = 0.5 and van der Waals = 0.5. Both force fields were computed using a Polak-Ribiere conjugate gradient method terminating when the root-mean-square gradient reached 0.001 kcal/(Å mol), and no cut-offs were applied. The energetic contributions to the total steric energy of the structures by bond stretching/compressing, bond angle deformations, torsional strain, van der Waals repulsions, hydrogen bonding, and electrostatic repulsions were all considered. Appropriate combinations of the energetically minimized structures were then merged to create drug–

polymer complexes. These complexes then underwent the same minimization procedures to determine whether they were energetically stabilized in relation to the individual components. This procedure is similar to that previously reported by Dott et al.<sup>22</sup>

Molecular attributes (specifically the surface area, volume and mass) of the energy-minimized structures were determined using the Quantitative Structure Activity Relationship (QSAR) option in HyperChem, where the surface area was determined using a grid method.

**Drug Release.** Dissolution tests were performed in 250 mL of phosphate buffered saline (PBS) (pH = 7.4) at 37 °C under continuous stirring on a magnetic stirrer. A total of 10 mg of fibers were added to the PBS solution, and at predefined time points, aliquots of 200 μL were withdrawn and the amount of drug determined with UV spectroscopy. For comparative purposes, the dissolution of the pure drug was also explored, using 2.3 mg of IMC or GSF (comparable with the intermediate formulations). The cumulative amount of drug released was calculated using a predefined calibration curve. The time lapse until complete disintegration of the fiber mat (assessed by visual inspection) was also recorded. Experiments were undertaken in triplicate. In all experiments, the maximum concentration of drug released was below the API solubility limit in PBS (IMC, 223.0 μg mL<sup>-1</sup>;<sup>23</sup> GSF, 14.2 μg mL<sup>-1</sup>).<sup>24</sup>

## RESULTS

**Ethanol/DMAc Solvent System.** Ethanol was initially explored as a solvent because a range of studies have used this to deliver successful ES processes.<sup>6</sup> However, the insolubility of GSF in ethanol meant that, although IMC materials could be prepared, no GSF fibers could be generated. The solvent system was thus changed to a 2:1 v/v mixture of ethanol and DMAc; this permitted GSF fibers to be prepared, but only with relatively low loadings of the drug. Details of the fibers prepared are given in Table 1 and SEM images in Figure 2. Attempts to elevate the GSF concentration in the fibers above 9.1% w/w were unsuccessful.

**Table 1. API-Loaded Fibers Prepared in 2:1 v/v Ethanol/DMAc<sup>a</sup>**

drug	ID	spinneret I.D. (mm)	fiber diameter (nm)	diameter uniformity (% RSD)
IMC	I1	0.84	221 ± 44	19.9
	I2	0.33	234 ± 88	37.6
GSF	G1	0.84	322 ± 77	23.9
	G2	0.33	366 ± 253	69.1

<sup>a</sup>Samples were prepared from 10 mL of a 1% w/v API solution to which 1000 mg of PVP was added, giving fibers which were 9.1% w/w API. The flow rate was 1 mL h<sup>-1</sup>.

In all cases, the fibers can be seen to have smooth, cylindrical morphologies. There is no evidence of “bead on string” morphology, nor can any particles be seen in the images. Possibly counterintuitively, the fibers from the 0.33 mm I.D. spinneret have slightly larger diameters than those from the 0.84 mm spinneret, although given the large standard deviations the sizes can be said to be essentially invariant with spinneret diameter. The GSF fibers are somewhat wider than the IMC materials, and use of the larger spinneret gives a more uniform size distribution. XRD and DSC analyses of the

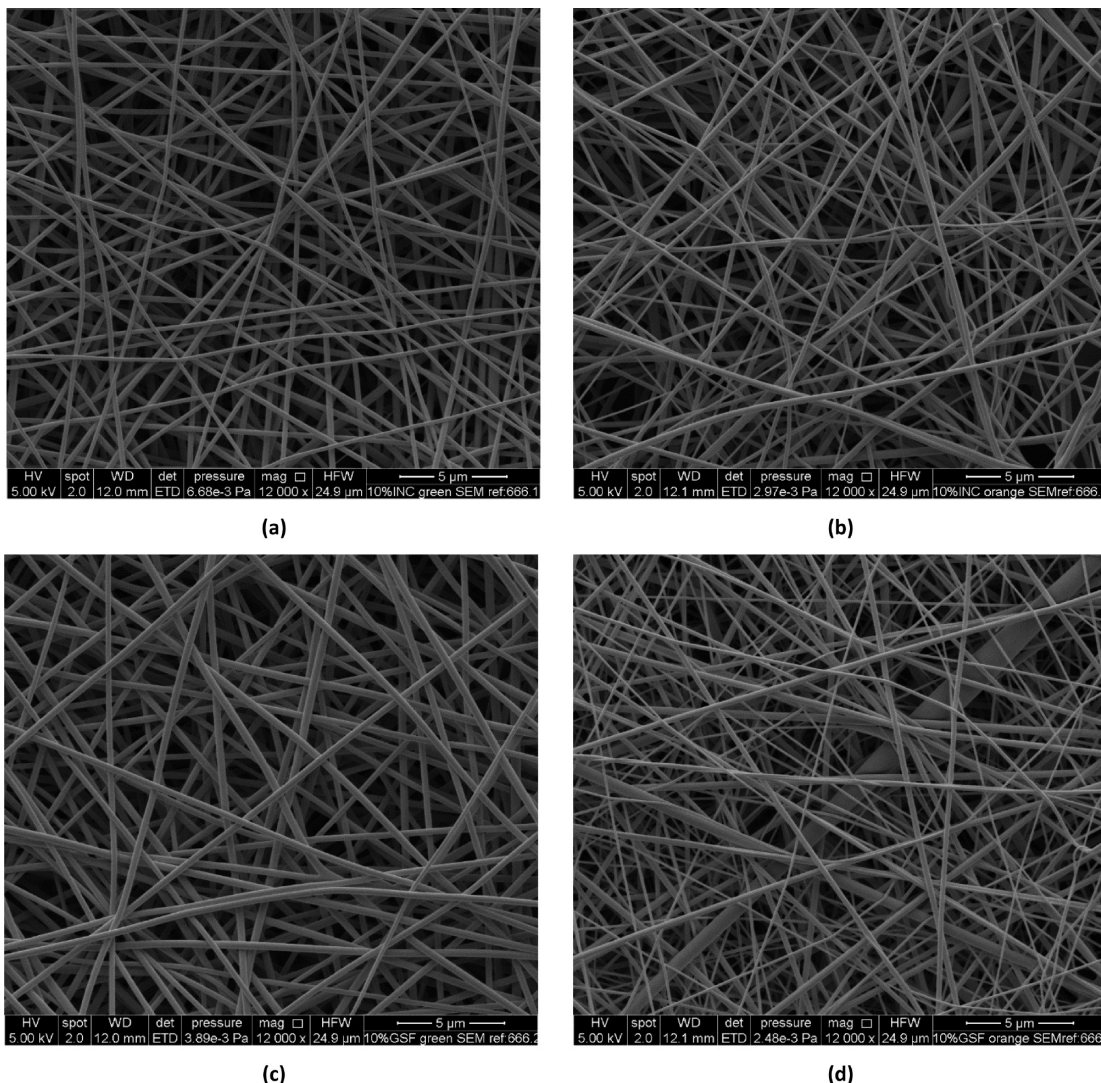


**Figure 2.** SEM images of (a) I1, (b) I2, (c) G1, and (d) G2.

fibers showed the drug to be in an amorphous physical state (see Supporting Information, Figures S1 and S2).

**Acetone/DMAc System. Process Optimization.** To prepare a useful formulation, drug loadings higher than 9% are often required; for IMC and GSF the standard doses are ca. 50–150 and 500–1000 mg per day depending on the indication and route of administration. Hence, a different solvent system from ethanol/DMAc was required. Acetone was selected to replace ethanol because of the higher solubility of GSF in the former. Because more uniform fiber diameters were seen with the 0.84 mm I.D. spinneret, this was employed for ES, with a flow rate of 1 mL h<sup>-1</sup> as used in previous experiments. A larger spinneret is likely to be particularly important when working with acetone, which evaporates very quickly and hence can cause the solidification of material on the spinneret, resulting in clogging. A larger spinneret should ameliorate this effect. Details of the formulations prepared are given in Table 2, and SEM images are in Figure 3.

As before, the fibers have uniform cylindrical morphologies, and there is no evidence for beading or the formation of API particles. There is no clear relationship between the drug loading and the fiber size, although it is clear that as for the ethanol/DMAc system the GSF fibers are less uniform in size

**Table 2. First Set of Fibers Prepared in 2:1 v/v Acetone/DMAc<sup>a</sup>**

drug	I.D.	API content <sup>b</sup> (% w/w)	fiber diameter (nm)	diameter uniformity (% RSD)
IMC	I3	9.1	389 ± 67	17.2
	I4	23.1	472 ± 85	18.0
GSF	G3	9.1	466 ± 151	32.4
	G4	23.1	268 ± 93	34.7

<sup>a</sup>Samples were prepared from 10 mL of a 1 or 3% w/v API solution to which 1000 mg of PVP was added. A spinneret with 0.84 mm I.D. was used for ES, with a 1 mL h<sup>-1</sup> flow rate. <sup>b</sup>The drug content in the fibers calculated from the relative masses of API and polymer.

than the IMC materials. Although this solvent system permitted a higher GSF loading to be realized, the process was observed to be rather capricious with frequent needle clogging occurring, particularly with higher GSF concentrations. The flow rate was thus increased to 2 mL h<sup>-1</sup> in the preparation of the final set of optimized fibers. Details of these can be found in Table 3. SEM images are shown in Figure 4.

Fibers could be prepared with higher concentrations of IMC, but attempts to make 37.5% w/w GSF fibers were unsuccessful,

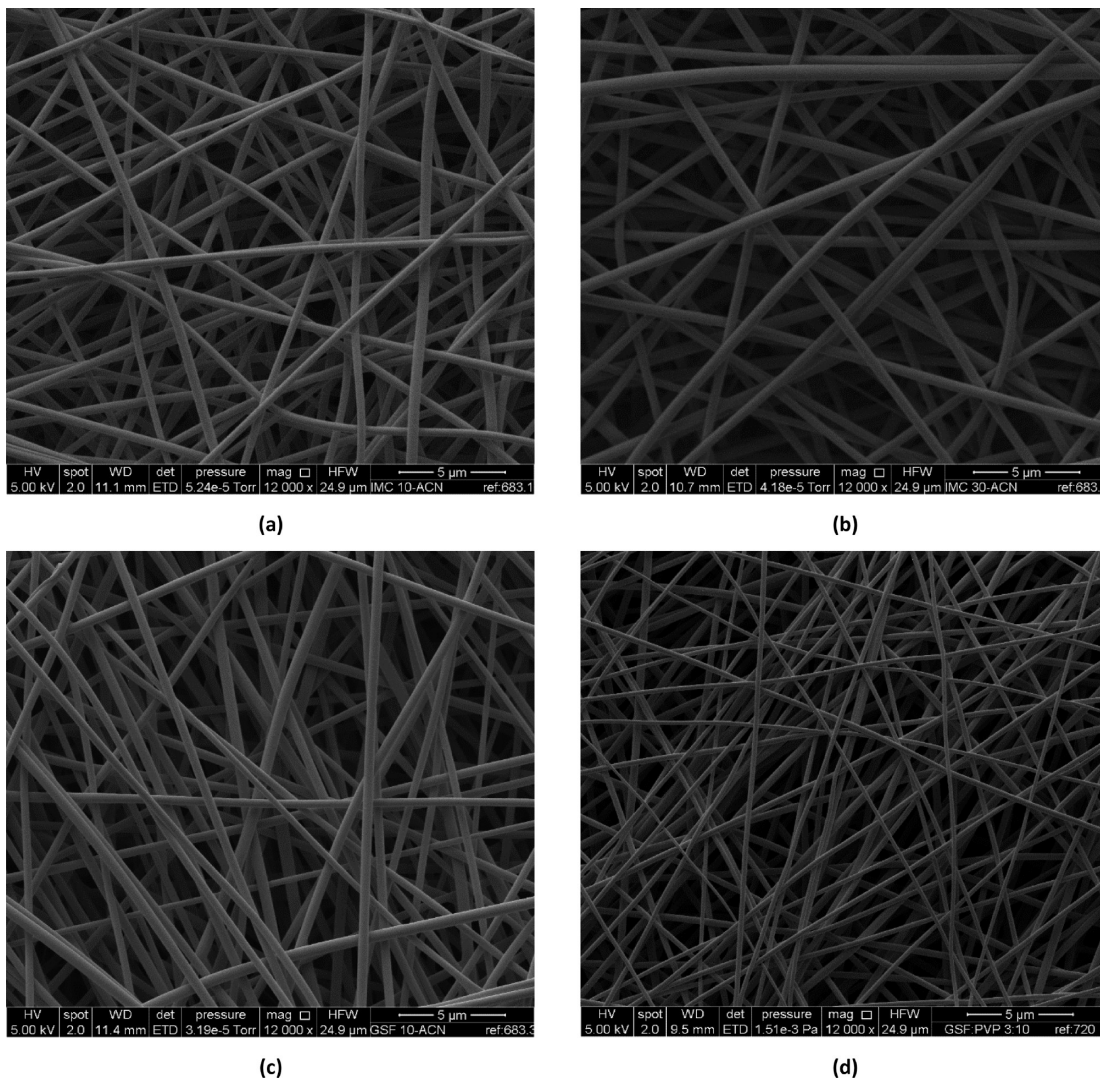


**Figure 3.** SEM images of (a) I3, (b) I4, (c) G3, and (d) G4.

**Table 3. Final Optimized Fibers Prepared in 2:1 v/v Acetone/DMAc<sup>a</sup>**

drug	I.D.	API content <sup>b</sup> (% w/w)	fiber diameter (nm)	diameter uniformity (% RSD)
IMC	I5	9.1	425 ± 134	31.4
	I6	16.7	510 ± 130	25.6
	I7	23.1	472 ± 164	34.9
	I8	28.6	631 ± 144	22.8
	I9	33.3	529 ± 143	26.9
GSF	G5	9.1	387 ± 132	34.4
	G6	16.7	564 ± 135	23.9
	G7	23.1	502 ± 156	30.9
	G8	28.6	523 ± 189	36.1
	G9	33.3	403 ± 168	41.5

<sup>a</sup>Samples were prepared from 10 mL of a 1–5% w/v API solution to which 1000 mg of PVP was added. A spinneret with 0.84 mm I.D. was used for ES, with a 2 mL h<sup>-1</sup> flow rate. <sup>b</sup>The drug content in the fibers calculated from the relative masses of API and polymer.

as the drug proved not to be sufficiently soluble under these conditions.

As for the previous sets of fibers, those depicted in Figure 4 have smooth cylindrical surfaces. It is clear from the images that

there appear to be two distinct populations of fibers, with some very fine fibers being observed. This effect is reflected in the large % RSDs seen for the size distributions. In some cases, morphological abnormalities in the form of rounded plates were also identified by SEM (see Supporting Information Figure S3); this is ascribed to be a result of the presence of residual solvent in the fiber mats after spinning. No clear trends between the drug loading and fiber size or size uniformity can be elucidated. The presence of residual solvent was confirmed by thermogravimetric analysis (Supporting Information Figure S4), in which a mass loss of ca. 11–12.5% is observed below 100 °C (attributed to water and acetone), followed by an additional 2.5–4.2% between 100 and 170 °C (believed to correspond to DMAc loss).

**Physical Form Characterization.** The optimized fiber sets I5–I9 and G5–G9 were investigated in detail using a range of solid state techniques. DSC data for selected materials are included in Figure 5.

The DSC traces clearly show the pure APIs to be crystalline materials, with distinct melting endotherms at 159 °C (IMC) and 209 and 218 °C (GSF). The observation of two peaks for the raw GSF material is a result of the melting of two different polymorphs, form I at 218 °C and either form II or III at 209 °C (the value observed is intermediate between those reported

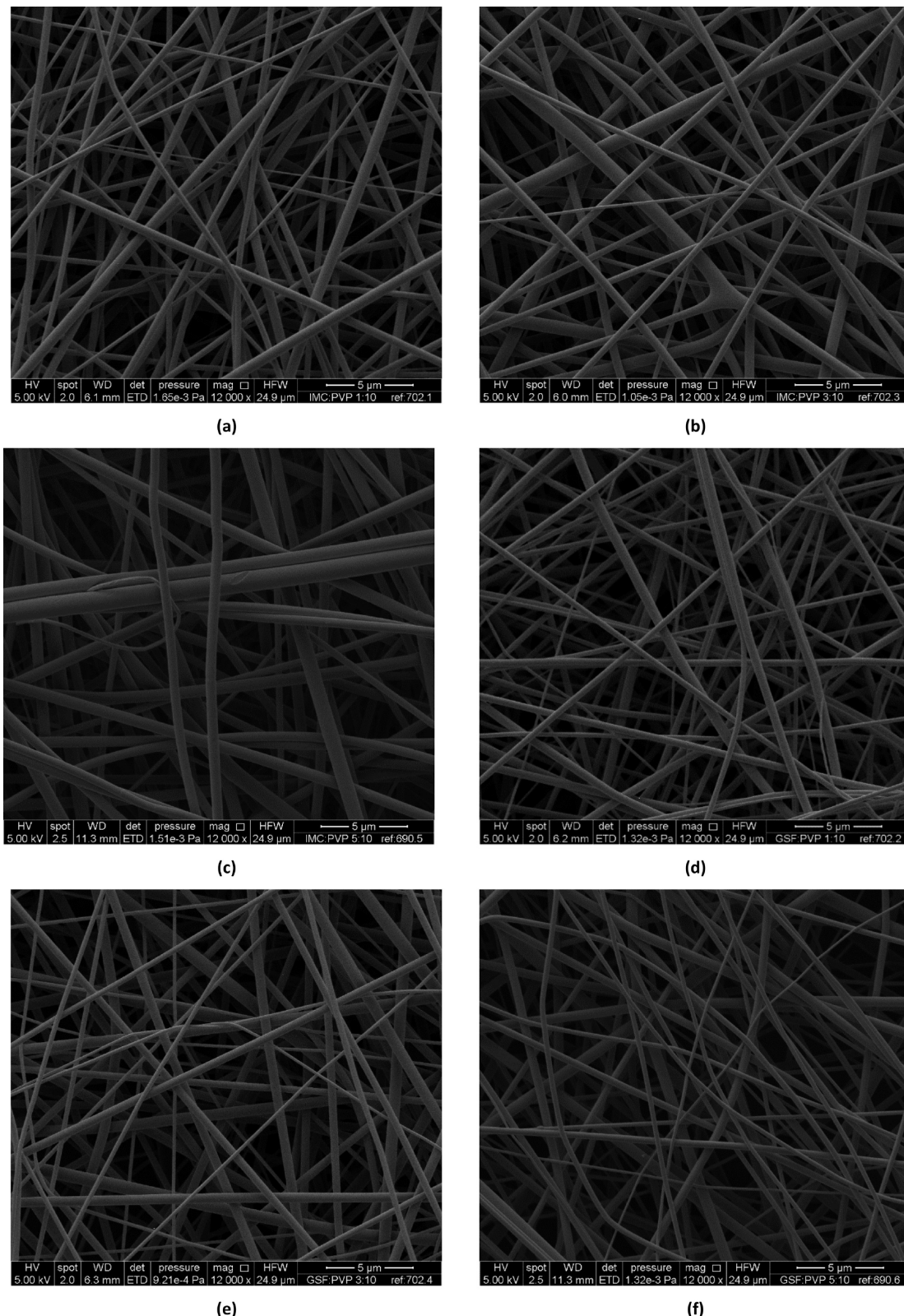
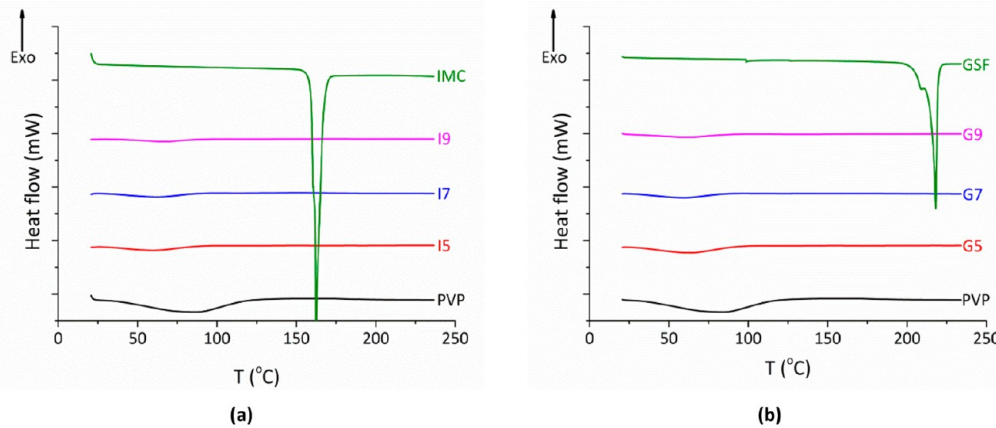


Figure 4. SEM images of (a) IS, (b) I7, (c) I9, (d) G5, (e) G7, and (f) G9.

in the literature for forms II and III).<sup>25</sup> In contrast, the PVP starting material is amorphous, exhibiting only a broad endotherm corresponding to dehydration below 125 °C and a glass transition temperature ( $T_g$ ) at around 180 °C. The DSC traces of all the drug-loaded fibers are typical of those of amorphous materials, with no indication of melting events and

only sub-100 °C dehydration endotherms being visible. This suggests that IMC and GSF are present in the amorphous physical form, regardless of the drug loading in the formulations. The assignment of the broad endotherm to dehydration was confirmed for selected samples by thermogravimetric analysis (Supporting Information Figure S4).



**Figure 5.** DSC data for selected electrospun fibers of (a) IMC and (b) GSF. Data were collected during a single heating cycle, with no preheating.

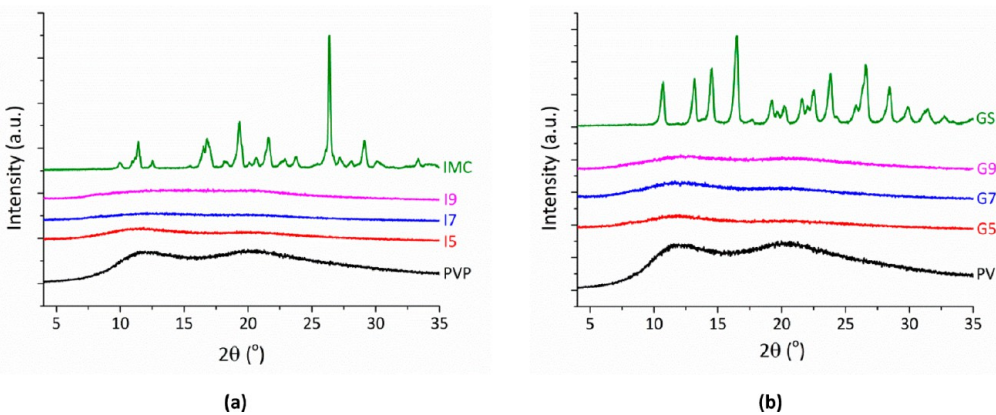


**Figure 6.** XRD data for selected electrospun fibers of (a) IMC and (b) GSF.

To investigate further the physical form of the drug in the fibers, X-ray diffraction (XRD) measurements were undertaken (Figure 6). Although the raw API powders exhibit numerous Bragg reflections, typical of crystalline materials, the patterns of PVP and all the electrospun formulations contain only the broad “haloes” expected for amorphous formulations. The XRD data, thus, agree well with the DSC results, confirming the amorphous physical state of the drug in the fibers.

**Drug–Polymer Interactions.** The interactions between the drug and polymer were investigated using both IR spectroscopy and modulated-temperature DSC. The IR spectra of IMC, GSF, and selected fibers are depicted in Figure 7.

As expected, the spectra of the fibers are largely composites of those of the raw materials. The major changes can be seen in the carboxylate region of the spectrum, where PVP has a distinct band at  $1654\text{ cm}^{-1}$  and IMC at  $1689$  and  $1712\text{ cm}^{-1}$ . In the spectra of I5–I9, the PVP and IMC bands have merged, and only a single broad band centered at  $1660\text{ cm}^{-1}$  (I5) or  $1664\text{ cm}^{-1}$  (I7, I9) is visible. In the spectrum of I9, a shoulder on this peak at ca.  $1720\text{ cm}^{-1}$  may be discerned. GSF shows a number of bands in the carboxylate region, with particularly notable peaks at  $1703$ ,  $1657$ ,  $1613$ ,  $1598$ , and  $1582\text{ cm}^{-1}$ . As was the case for IMC fibers, the GSF bands are merged together with the PVP C=O peak in G5, with a main peak at  $1663\text{ cm}^{-1}$  and shoulders at  $1614$  and  $1589\text{ cm}^{-1}$ . The latter peaks increase in intensity as the GSF content increases and move to lower wavenumber (G7, 1613 and  $1588\text{ cm}^{-1}$ ; G9, 1612 and  $1588\text{ cm}^{-1}$ ), whereas the major peak at  $1663\text{ cm}^{-1}$  is shifted to around  $1658\text{ cm}^{-1}$  in G9. The shifts in peak positions

observed in the IMC and GSF fibers may be a result of interactions (e.g., van der Waals) between the API and PVP components of the fibers or, alternatively, could be a result of the crystalline physical form having become amorphous as a result of fiber formation. The more significant changes observed in the IR spectrum of the IMC fibers might be indicative of greater drug/polymer interactions in this case, but this cannot be confirmed from IR spectroscopy alone.

Modulated temperature DSC (MT-DSC) was employed to determine the glass transition temperatures ( $T_g$ ) of the materials and provide additional insight into the interaction between the API and polymer. MT-DSC is much more powerful than standard DSC for accurate  $T_g$  determination because it permits the reversible and nonreversible components of the heat flow to be deconvoluted.<sup>26</sup> If the two components in a binary mixture undergo ideal mixing, then the composite will show a single  $T_g$  which can be calculated theoretically from the mass composition of the mixture using the Fox equation<sup>27</sup>

$$\frac{1}{T_g^{\text{composite}}} = \frac{w_1}{T_g^1} + \frac{w_2}{T_g^2}$$

where  $w_1$  and  $w_2$  are the mass fractions of the two materials in the mixture. The Gordon–Taylor equation may alternatively be used

$$\frac{1}{T_g^{\text{composite}}} = \frac{w_1 + Kw_2}{w_1 T_g^1 + Kw_2 T_g^2}$$

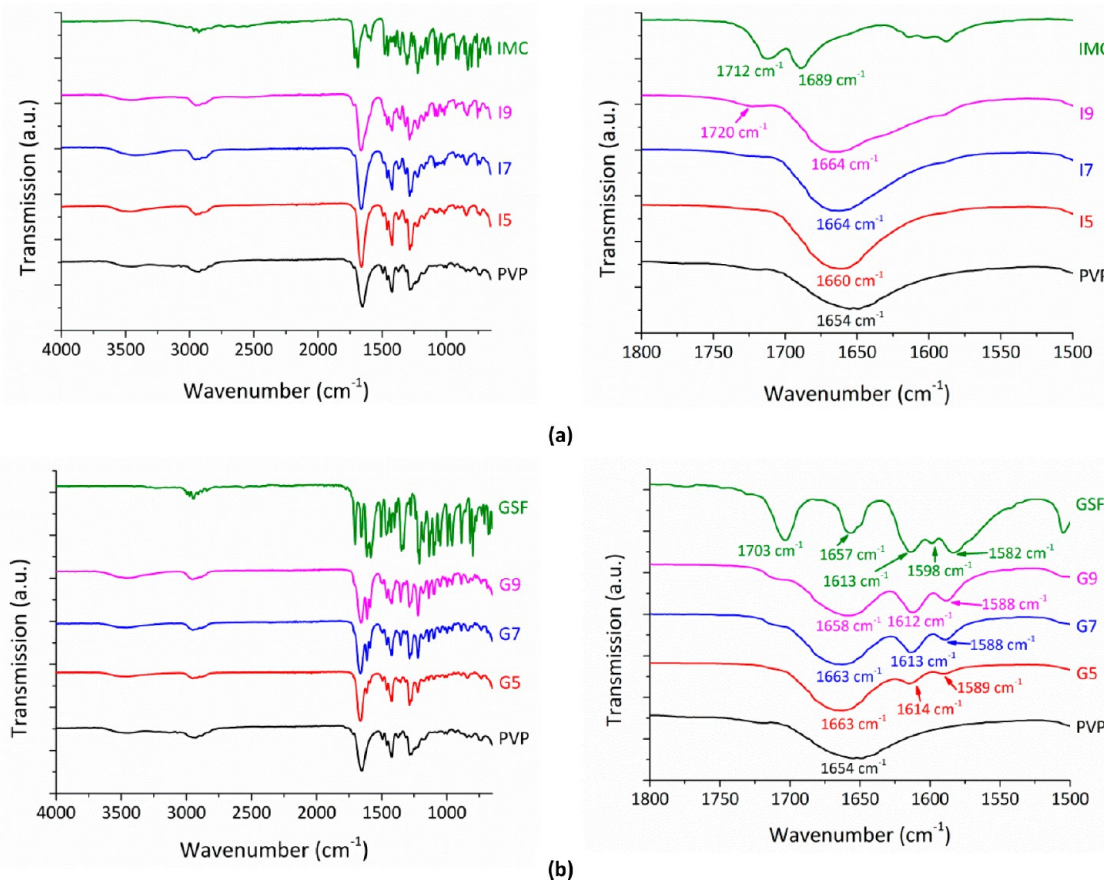


**Figure 7.** IR spectra for the raw materials and electrospun fibers of (a) IMC and (b) GSF. The full spectrum is shown on the left, and an enlargement of the 1800–1500  $\text{cm}^{-1}$  region to the right.

This additionally includes a constant  $K$ . A number of approaches have been used to calculate the value of  $K$ , including from the  $T_g$  of the two components and their densities,<sup>5</sup> from specific heat capacities,<sup>27</sup> or empirically.<sup>28</sup> MT-DSC was employed to determine the experimental  $T_g$  values for the drug-loaded nanofibers I5–I9 and G5–G9 within 48 h of preparation. The results are given in Table 4 (selected raw data may be found in Supporting Information Figure S5). Both the Fox and Gordon–Taylor equations were fitted to the data, and the results are in Figure 8.

In both cases, it can be seen that the Fox equation provides a poor fit to the observed data, predicting higher values for  $T_g$  than are seen experimentally. The difference is more marked in the case of GSF. The Gordon–Taylor equation could satisfactorily be used to fit the experimental data, with  $K$  values of  $0.60 \pm 0.01$  for IMC and  $0.51 \pm 0.02$  for GSF ( $K$  was determined by nonlinear least-squares fitting, and the uncertainties are those calculated from the fitting process). It has previously been reported that higher  $K$  values are observed with increased intermolecular interactions,<sup>31</sup> and thus, the MT-DSC data appear to confirm the presence of increased polymer/API interactions with IMC as indicated in IR spectroscopy.

**Molecular Modeling.** To gain more insight into the drug–polymer interactions in the electrospun fibers, molecular models of IMC, GSF, PVP, PVP-IMC, and PVP-GSF were constructed using the HyperChem software. The structures of a PVP decamer and the APIs were first individually optimized, and subsequently, appropriate combinations of the energetically

**Table 4.**  $T_g$  Values for Fibers I5–I9 and G5–G9 As Determined by MT-DSC<sup>a</sup>

drug	fiber I.D.	$T_g$ ( $^{\circ}\text{C}$ )		
		fresh sample	after 4 months	after 8 months
IMC	pure PVP	181.58	NM	NM
	PVP fibers	180.61	NM	NM
	pure drug <sup>a</sup>	46.05	NM	NM
	I5	159.51	157.48	157.16
	I6	146.86	140.39	141.22
	I7	134.44	137.58	134.71
GSF	I8	127.85	123.99	124.10
	I9	119.79	114.88	116.82
	pure drug <sup>a</sup>	91.74	NM	NM
	G5	163.25	165.41	164.40
	G6	155.31	155.75	156.68
	G7	147.24	147.38	148.53
	G8	141.96	140.54	140.52
	G9	137.98	137.99	137.13

<sup>a</sup> $T_g$  values of the pure drugs were obtained from amorphous IMC and GSF samples prepared by quench cooling. The observed values agree well with the literature, which records values of 42  $^{\circ}\text{C}$  for IMC,<sup>29</sup> and 89  $^{\circ}\text{C}$  for GSF.<sup>30</sup> NM = not measured.

minimized structures were merged to create drug–polymer complexes. The drug comprises 24.4% (IMC) or 24.1% (GSF) w/w in these complexes; thus, they are representative of the middle of the composition range studied experimentally. Figure 9 shows the geometric preferences for the energetically

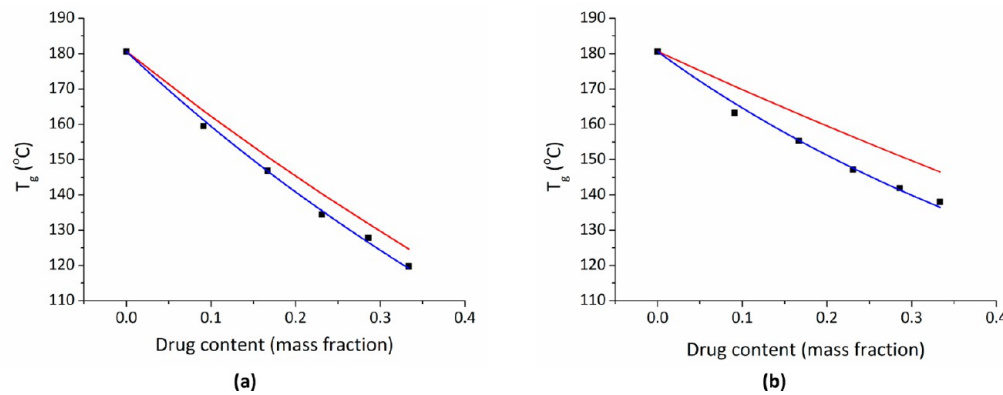


**Figure 8.**  $T_g$  data for (a) the IMC fibers I5–I9 and (b) the GSF G5–G9 materials. Experimental data are shown as black squares, values calculated using the Fox equation as a red line, and least-squares fitting of the Gordon–Taylor equation as a blue line.

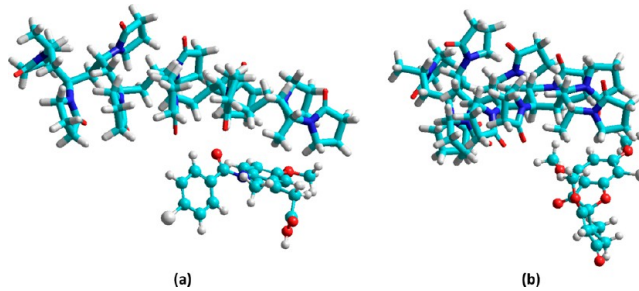


**Figure 9.** Optimized geometric arrangements of a PVP decamer with (a) IMC and (b) GSF. The PVP decamer can be seen at the top of the images, and the drug molecule at the bottom.

minimized API–polymer complexes. The energetic contributions to the overall steric energy for both the drug–polymer complexes and the individual API molecules and PVP decamer are given in Table 5. Stabilization of the complexes is indicated by a negative difference ( $\Delta E$ ) between the total steric energy of the complex and the sum of the total steric energies of the individual molecules.

The data from Table 5 reveal that the combined steric energy of PVP and GSF is 142.99 kcal mol<sup>-1</sup>, whereas the energy of the optimized complex is 133.03 kcal mol<sup>-1</sup>. This gives a  $\Delta E$  of -9.96 kcal mol<sup>-1</sup>, clearly demonstrating that there are interactions between the drug and polymer. For PVP-IMC, the combined energy of the components is 144.96 kcal mol<sup>-1</sup>, whereas that of the optimized geometry complex is 125.99 kcal mol<sup>-1</sup>, a  $\Delta E$  of -18.97 kcal mol<sup>-1</sup>. The drug/polymer interactions are therefore much stronger with PVP-IMC than with PVP-GSF, confirming the results observed in IR spectroscopy and MT-DSC. QSAR properties were also determined (see Supporting Information Table S1), and match the results from the geometry optimization: the surface

area to volume ratio is lower and the density higher for the PVP-IMC complex than for the PVP-GSF complex.

**Stability Studies.** It is clear that immediately after synthesis, the drug is present in the fibers in the amorphous physical form. However, when formulating amorphous APIs the issue of relaxation to a crystalline state is a major concern. The stability of the formulations, thus, was investigated by DSC and MT-DSC after 4 months' storage in a desiccator over silica gel. Representative data sets are given in Supporting Information Figures S6 and S7, respectively. No melting endotherms were visible in any of the DSC thermograms. Clear  $T_g$  events were observed in MT-DSC, however. The  $T_g$  values after aging are very similar to those seen with fresh samples (see Table 4). The  $K$ -values calculated using the Gordon–Taylor equation are also little changed:  $0.54 \pm 0.03$  for IMC and  $0.51 \pm 0.01$  for GSF. These data demonstrate that both IMC and GSF remain in the amorphous physical state over a prolonged period of time in the ES fibers. The lack of crystallization over this time is consistent with the APIs being present as a solid solution with interactions between them and the polymer, rather than forming a solid suspension containing amorphous particles; crystallization is expected to be much more rapid in the latter case. It appears that for I9 there are two  $T_g$  events after storage; one at 114.88 °C and one at around 173 °C. The latter value is close to that determined for pure PVP and may be indicative of some phase separation occurring. Two  $T_g$ s are also visible in the DSC data for G7 (one at 147.38 °C and the other ca. 185 °C), which might again be the result of some phase separation.

TGA and MT-DSC data were also obtained after storage for 8 months in a desiccator. The TGA data for selected samples are presented in Supporting Information Figure S8. It can be seen that the mass loss profiles are very different from those recorded for fresh samples, with mass losses below 100 °C being around 2–5.3% with the IMC-loaded fibers and 3.6–

**Table 5. Details of the Energetics of the Optimized Geometries in the PVP–Drug Molecular Models<sup>a</sup>**

species	minimized energy contributions (kcal mol <sup>-1</sup> )					
	bond stretching	bond angle	torsional	van der Waals	hydrogen bonding	total
IMC	0.616	12.78	7.477	3.834	$-1.057 \times 10^{-5}$	24.707
GSF	1.143	16.489	3.665	1.439	0	22.735
PVP	4.337	82.689	46.017	-12.788	0	120.255
PVP-IMC	4.772	94.927	52.04	-25.753	$-1.481 \times 10^{-5}$	125.992
PVP-GSF	5.279	101.954	48.118	-22.321	0	133.030

<sup>a</sup>The electrostatic contribution was zero in all cases.

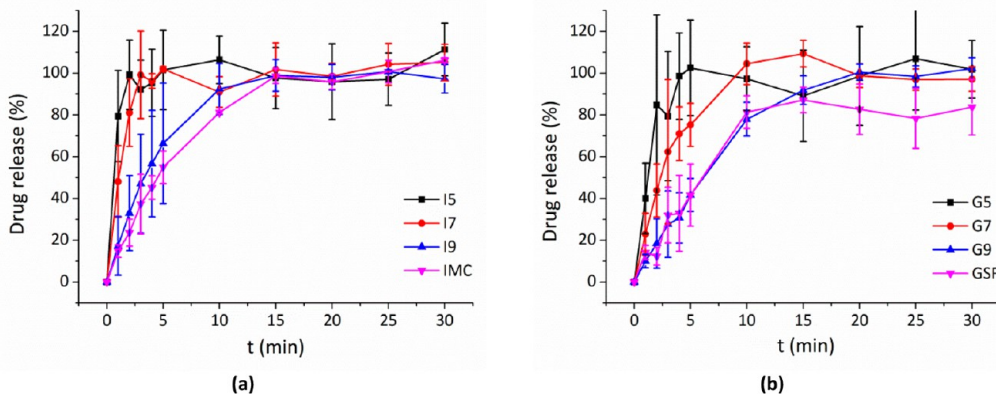


**Figure 10.** Drug release data for the formulations (a) I5, I7, and I9 and (b) G5, G7, and G9. Data are from three independent experiments and are given as mean  $\pm$  SD.

6.6% for the GSF/PVP materials. Higher drug loadings appear to result in decreased solvent loss below 100 °C. Mass losses between 100 and 170 °C are between 0.7 and 1.1% for all samples, with no clear correlation between this and the drug loading. MT-DSC data are given in Supporting Information Figure S9, with the accompanying  $T_g$  values in Table 4. It can be seen that  $T_g$  remains essentially unchanged after 8 months' storage. The Gordon–Taylor equation can again be fitted to the experimental values, yielding  $K$  values of  $0.54 \pm 0.02$  and  $0.51 \pm 0.01$  for IMC and GSF, respectively. These values are very similar to those determined for fresh fibers and after four months' storage. There is some evidence for phase separation again, with two  $T_g$  values visible for I6, I8, and G9 (the second at 181.97, 182.32, and 180.84 °C, respectively). As previously, no melting events could be observed by DSC, confirming the presence of amorphous drug.

Thus, it appears clear from the aging data that, although the solvent content of the fibers declines with time and some phase separation is observed after aging, the APIs remain in an amorphous state even after prolonged periods of storage.

**Functional Performance Studies.** The pharmaceutical functionality of the fibers was assessed by monitoring the time taken for the fiber mat to disintegrate and by dissolution testing. The data obtained are summarized in Figure 10 and Table 6.

It is clear from the above data that the fiber mats disintegrate very quickly, in less than 20 min, with the disintegration time increasing with drug loading for both APIs. Drug release is similarly rapid, also being complete within 20 min. As a result

of the very quick dissolution processes, the error bars in the measurements are large, but the general trends are nevertheless obvious: an increase in drug loading leads to a slower release process. The lower drug-loading fibers all exhibit a markedly increased dissolution rate over the pure drug. The amount of pure drug used for the control experiments correlates with the amount in the I7/G7 fibers. Thus, although in percentage terms, the G9 fibers (which contain the most drug [33.3% w/w]) are observed to release the drug at approximately the same rate as pure GSF dissolves and the I9 fibers appear to dissolve only slightly faster than the pure drug, in concentration terms, dissolution is accelerated in both cases.

The very rapid release of drug precludes a detailed kinetic analysis, and for I5, I7, G5, and G7 there is too little data to fit kinetic models. For I9 and G9, it proved possible to fit the Korsmeyer–Peppas model ( $M_t/M_{\infty} = kt^n$ , where  $k$  is a rate constant,  $t$  is the time elapsed, and  $n$  is an exponent giving information on the release mechanism) to the data (Figure 11),

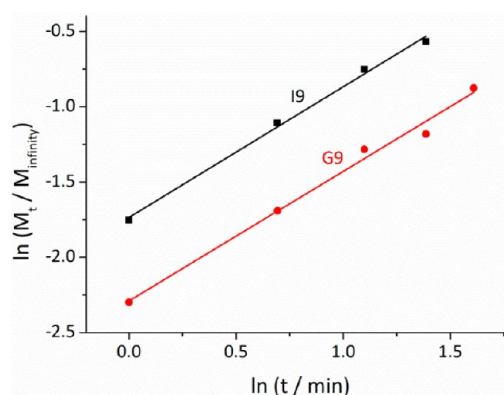


**Figure 11.** Fits of the Korsmeyer–Peppas model to drug release from I9 and G9.

but caution must be taken in drawing detailed conclusions owing to the small number of data points where the percentage release was below 60%. The value of the rate constant was determined to be ca.  $0.18 \text{ min}^{-1}$  for I9 and  $0.10 \text{ min}^{-1}$  for G9; these are identical within the error of the experiment, suggesting that it is the properties of the polymer rather than the drug which control the release rate. The value of the  $n$  exponent is 0.87 for I9 and 0.86 for G9, indicating that in both cases anomalous transport (i.e., non-Fickian mass transfer) governs the release rate (the systems exist as polymer films).<sup>32</sup>

**Table 6. Summary of the Pharmaceutical Characteristics of the IMC and GSF Fibers<sup>a</sup>**

drug	fiber I.D.	disintegration time (min)	$t_{100}$ (min) <sup>b</sup>
IMC	pure drug		$16.67 \pm 2.89$
	I5	$1.7 \pm 0.8$	$1.7 \pm 0.6$
	I7	$4.8 \pm 1.9$	$4.3 \pm 1.2$
	I9	$11.0 \pm 6.0$	$10.0 \pm 5.0$
GSF	pure drug		NR
	G5	$3.3 \pm 1.0$	$3.3 \pm 1.2$
	G7	$8.5 \pm 2.2$	$7.7 \pm 4.0$
	G9	$16.7 \pm 1.5$	$18.3 \pm 2.8$

<sup>a</sup>Data are from three independent experiments and are given as mean  $\pm$  S.D. <sup>b</sup> $t_{100}$  is the time taken for 100% drug release to be obtained. NR = not reached.

## ■ DISCUSSION

From the work undertaken in this study, it is clear that the solvent used for electrospinning of indomethacin (IMC) and griseofulvin (GSF), the size of needle used for spinning, flow rate, and the drug loading are all important factors influencing the results obtained. Generally, it has been observed that a narrower needle results in a more polydisperse distribution of fiber sizes and also in increased clogging. When spinning using the ethanol/DMAc solvent system at 1 mL h<sup>-1</sup>, higher drug loadings also result in a broader distribution of fiber diameters, but in acetone/DMAc, there is no clear trend between drug loading and uniformity of size.

A number of sets of electrospinning processing parameters were explored, and in order to obtain usefully high loadings of the poorly soluble GSF, it was found necessary to use a mixture of acetone and DMAc as the solvent system. With this system, clogging was observed to occur with a (relatively slow) flow rate of 1 mL h<sup>-1</sup>, and hence, the dispensing rate was increased to 2 mL h<sup>-1</sup>; this ameliorated the issue with clogging, but did in some cases result in evidence being seen for solvent droplet incorporation in the fiber mat. Using acetone/DMAc and a flow rate of 2 mL h<sup>-1</sup>, two series of five different PVP–drug fibers were produced, one containing GSF and the other IMC. Upon manufacturing, no evidence for polymer/drug phase separation was seen with any of the fibers, all of which were observed to be smooth and cylindrical by electron microscopy, with no evidence for any secondary particles. In all cases, the drug existed in the fibers in the amorphous physical form, as shown using X-ray diffraction and differential scanning calorimetry. The fibers released the embedded drug very rapidly, within 20 min, with the fibers offering enhanced dissolution rates compared to the pure drugs alone. These findings suggest that the electrospun fibers prepared in this work may have significant potential for fast-dissolving buccal or sublingual drug delivery.

FT-IR spectroscopy and modulated temperature DSC (MT-DSC) were used to probe the interactions between the drug and the polymer. Some shifts in peak positions were observed between the crystalline drug and the fiber formulations in IR spectra, which may be a result of intermolecular forces or of the changes in the drugs' physical forms. The MT-DSC showed that the  $T_g$  values of neither set of fibers obeyed the Fox equation, but both could be modeled using the Gordon–Taylor model. To the best of our knowledge this is only the second time that either the Gordon–Taylor or the Fox equation have been applied to ES fibers.<sup>5,33</sup> The APIs in the fibers were found to remain amorphous after 4 and 8 months of storage.

The deviation from the Fox equation observed with both APIs may be a result of the nature of the interactions between the polymer and the drug<sup>27</sup> or could mean that rather than forming a perfect solid solution, the drug is present at least in part as a solid suspension. The fact that the material remained amorphous after 4 or 8 months' of storage suggests that the former may be the more likely explanation (if drug particles were present, we would expect crystallization). The Gordon–Taylor  $K$  parameter calculated for the GSF fibers is lower than that determined for IMC, which is indicative of reduced interactions between drug and polymer in the GSF formulations cf. their IMC analogues.<sup>31</sup> The construction of a simple molecular model showed that the optimized geometry for a PVP–IMC complex has a  $\Delta E$  of  $-18.97$  kcal mol<sup>-1</sup>, whereas PVP–GSF has  $\Delta E = -9.96$  kcal mol<sup>-1</sup>. This, together

with QSAR calculations of a reduced surface area-to-volume ratio and greater density in the former case, confirms the greater strength of the PVP–IMC intermolecular forces.

This hypothesis is also supported by the literature. The formation of bonding interactions between IMC and PVP has been demonstrated by Xiang and Anderson using molecular dynamics simulations.<sup>34</sup> Vasanthavada et al. prepared drug–PVP solid dispersions and observed intermolecular interactions between PVP and indoprofen (a drug with structural similarities to IMC), but not between GSF and PVP.<sup>35</sup> We can thus safely conclude that there are greater interactions with PVP in the IMC-loaded fibers.

Our results are in good agreement with the bulk of the literature,<sup>6,16,18–20</sup> in that we observe the formation of amorphous API dispersions in all the electrospun fibers studied. This is in contrast to the findings of Taepaiboon et al., who observed crystalline IMC in their IMC/PVA fibers at 16.7% w/w.<sup>15</sup> The difference is presumably a result of these authors using water, in which IMC is poorly soluble, as a solvent for their experiments. The stability of the amorphous physical form observed here is fully in agreement with the work of Blair et al., who observed that IMC in IMC/PVP fibers remained amorphous after up to 6 months' storage in a desiccator at 40 °C.<sup>18</sup>

In this work, no major differences between the behavior of the GSF and IMC materials were observed. Despite the latter forming much more stable glasses, both APIs were successfully converted into the amorphous physical form by electrospinning even at the highest drug loadings (33.3% w/w) and remained in this state after storage for 8 months. The drug loadings studied were limited by the solubility of GSF in the acetone/DMAc solvent solution, but we did not observe any greater tendency to crystallinity for the GSF materials. Our findings, thus, suggest that electrospinning can successfully render even the poorest glass-formers amorphous and, hence, is a powerful technique for the production of fast dissolving formulations.

## ■ CONCLUSIONS

Electrospun fibers of polyvinylpyrrolidone and indomethacin (IMC) or griseofulvin (GSF) were successfully prepared in this study. By suitable selection of the processing parameters, it proved possible to load both drugs in the fibers up to 33.3% w/w. All the fibers prepared were smooth and cylindrical and contained the drug in an amorphous physical form, which remains stable over the 8-month time period. FT-IR spectroscopy, modulated temperature differential scanning calorimetry, and molecular modeling showed that there were interactions between the drug and polymer with both IMC and GSF; these are much stronger in the IMC case. All the fibers were found to release the drug very rapidly, demonstrating accelerated dissolution over the pure drug. This study, thus, indicates that the electrospinning process is able, by dint of the very rapid evaporation of solvent that occurs therein, to render even drugs that form highly unstable glasses into the amorphous form and retain them in that metastable state for prolonged periods of time.

## ■ ASSOCIATED CONTENT

### Supporting Information

The results of QSAR calculations for the drug/polymer composites; DSC and XRD data for fibers prepared from ethanol/DMAc; additional SEM images for fibers generated from acetone/DMAc; TGA and MT-DSC data recorded both

immediately after sample preparation and after aging; and DSC data for aged fibers. This material is available free of charge via the Internet at <http://pubs.acs.org>.

## AUTHOR INFORMATION

### Corresponding Authors

\*E-mail: s.gaisford@ucl.ac.uk. Tel.: +44 (0) 20 7753 5853.

\*E-mail: g.williams@ucl.ac.uk. Tel.: +44 (0) 207 753 5868.

### Notes

The authors declare no competing financial interest.

## ACKNOWLEDGMENTS

F.L.L. thanks the EPSRC for a Ph.D. studentship under the CDT in Targeted Therapeutics & Formulation Sciences (EP/I01375X/1). The authors would also like to thank David McCarthy for SEM images and Drs. Bahijja Raimi-Abraham and Asma Buanz for help with TGA experiments.

## REFERENCES

- (1) Gaisford, S.; Saunders, M. *Essentials of Pharmaceutical Preformulation*; Wiley-Blackwell: Hoboken, NJ, 2013.
- (2) Arinstein, A.; Zussman, E. Postprocesses in tubular electrospun nanofibers. *Phys. Rev. E* **2007**, *76*, 056303.
- (3) Wu, X. F.; Salkovkiy, Y.; Dzenis, Y. A. Modeling of solvent evaporation from polymer jets in electrospinning. *Appl. Phys. Lett.* **2011**, *98*, 223108.
- (4) Illangakoon, U. E.; Nazir, T.; Williams, G. R.; Chatterton, N. P. Mebeverine-loaded electrospun nanofibers: physicochemical characterization and dissolution studies. *J. Pharm. Sci.* **2014**, *103* (1), 283–92.
- (5) Verreck, G.; Chun, I.; Peeters, J.; Rosenblatt, J.; Brewster, M. E. Preparation and characterization of nanofibers containing amorphous drug dispersions generated by electrostatic spinning. *Pharm. Res.* **2003**, *20* (5), 810–817.
- (6) Yu, D.-G.; Yu, X.-F.; Zhang, X.-X.; Shen, C.; Brandford White, L.-M. Ultrafine ibuprofen-loaded polyvinylpyrrolidone fiber mats using electrospinning. *Polym. Int.* **2009**, *58* (9), 1010–1013.
- (7) Alhusein, N.; Blagbrough, I. S.; De Bank, P. A. Zein/polycaprolactone electrospun matrices for localised controlled delivery of tetracycline. *Drug Delivery Transl. Res.* **2013**, *3* (6), 542–550.
- (8) Alhusein, N.; De Bank, P. A.; Blagbrough, I. S.; Bolhuis, A. Killing bacteria within biofilms by sustained release of tetracycline from triple-layered electrospun micro/nanofibre matrices of polycaprolactone and poly(ethylene-co-vinyl acetate). *Drug Delivery Transl. Res.* **2013**, *3* (6), 531–541.
- (9) Williams, G. R.; Chatterton, N. P.; Nazir, T.; Yu, D.-G.; Zhu, L.; Brandford-White, C. J. Electrospun nanofibers in drug delivery: recent developments and perspectives. *Ther. Delivery* **2012**, *3* (4), 515–533.
- (10) Natu, M. V.; de Sousa, H. C.; Gil, M. H. Effects of drug solubility, state and loading on controlled release in bicomponent electrospun fibers. *Int. J. Pharm.* **2010**, *397* (1–2), 50–8.
- (11) Vyazovkin, S.; Dranca, I. Physical stability and relaxation of amorphous indomethacin. *J. Phys. Chem. B* **2005**, *109*, 18637–18644.
- (12) Zhou, D.; Zhang, G. Z.; Law, D.; Grant, D. J. W.; Schmitt, E. A. Thermodynamics, molecular mobility and crystallization kinetics of amorphous griseofulvin. *Mol. Pharmaceutics* **2008**, *5* (6), 927–936.
- (13) Nagy, Z. K.; Nyul, K.; Wagner, I.; Molnar, K.; Marosi, G. Electrospun water soluble polymer mat for ultrafast release of Donepezil HCl. *eXPRESS Polym. Lett.* **2010**, *4* (12), 763–772.
- (14) Vrbata, P.; Berka, P.; Stranska, D.; Dolezal, P.; Musilova, M.; Cizinska, L. Electrospun drug loaded membranes for sublingual administration of Sumatriptan and naproxen. *Int. J. Pharm.* **2013**, *457* (1), 168–76.
- (15) Taepaiboon, P.; Rungsardthong, U.; Supaphol, P. Drug-loaded electrospun mats of poly(vinyl alcohol) fibres and their release characteristics of four model drugs. *Nanotechnol.* **2006**, *17* (9), 2317–2329.
- (16) Pornopone, V.; Supaphol, P.; Rangkupan, R.; Tantayanon, S. Electrospun methacrylate-based copolymer/indomethacin fibers and their release characteristics of indomethacin. *J. Polym. Res.* **2006**, *14* (1), 53–59.
- (17) Tungprapa, S.; Jangchud, I.; Supaphol, P. Release characteristics of four model drugs from drug-loaded electrospun cellulose acetate fiber mats. *Polymer* **2007**, *48* (17), 5030–5041.
- (18) Brettmann, B. K.; Myerson, A. S.; Trout, B. L. Solid-state nuclear magnetic resonance study of the physical stability of electrospun drug and polymer solid solutions. *J. Pharm. Sci.* **2012**, *101* (6), 2185–93.
- (19) Brettmann, B.; Bell, E.; Myerson, A.; Trout, B. Solid-state NMR characterization of high-loading solid solutions of API and excipients formed by electrospinning. *J. Pharm. Sci.* **2012**, *101* (4), 1538–45.
- (20) Rasekh, M.; Karavasil, C.; Soong, Y. L.; Bouropoulos, N.; Morris, M.; Armitage, D.; Li, X.; Fatouros, D. G.; Ahmad, Z. Electrospun PVP-indomethacin constituents for transdermal dressings and drug delivery devices. *Int. J. Pharm.* **2014**, *473* (1–2), 95–104.
- (21) Wang, L.; Wang, M.; Topham, P. D.; Huang, Y. Fabrication of magnetic drug-loaded polymeric composite nanofibres and their drug release characteristics. *RSC Adv.* **2012**, *2* (6), 2433.
- (22) Dott, C.; Tyagi, C.; Tomar, L. K.; Choonara, Y. E.; Kumar, P.; du Toit, L. C.; Pillay, V. A Mucoadhesive Electrospun Nanofibrous Matrix for Rapid Oramucosal Drug Delivery. *J. Nanomater.* **2013**, 924947.
- (23) El-Badry, M.; Fetih, G.; Fathy, M. Improvement of solubility and dissolution rate of indomethacin by solid dispersions in Gelucire 50/13 and PEG4000. *Saudi Pharm. J.* **2009**, *17* (3), 217–25.
- (24) Mosharraf, M.; Nystrom, C. The effect of dry mixing on the apparent solubility of hydrophobic, sparingly soluble drugs. *Eur. J. Pharm. Sci.* **1999**, *9*, 145–156.
- (25) Mahieu, A.; Willart, J.-f.; Dudognon, E.; Eddleston, M. D.; Jones, W. On the polymorphism of griseofulvin: Identification of two additional polymorphs. *J. Pharm. Sci.* **2013**, *102* (2), 462–468.
- (26) Verdonck, E.; Schaap, K.; Thomas, L. C. A discussion of the principles and applications of modulated temperature DSC (MTDSC). *Int. J. Pharm.* **1999**, *192* (1), 3–20.
- (27) An, L.; He, D.; Jing, J.; Wang, Z.; Yu, D.; Jiang, B. Effects of molecular weight and interaction parameter on the glass transition temperature of polystyrene mixtures and its blends with polystyrene/poly (2,6-dimethyl-p-phenylene oxide). *Eur. Polym. J.* **1997**, *33* (9), 1523–1528.
- (28) Seo, J.-A.; Oh, J.; Kim, H. K.; Hwang, Y.-H. Study of glass transition temperatures in sugar mixtures. *J. Korean Phys. Soc.* **2005**, *46* (3), 606–609.
- (29) Chokshi, R. J.; Shah, N. H.; Sandhu, H. K.; Malick, A. W.; Zia, H. Stabilization of low glass transition temperature indomethacin formulations: Impact of polymer-type and its concentration. *J. Pharm. Sci.* **2008**, *97* (6), 2286–2298.
- (30) Al Obaidi, H.; Buckton, G. Evaluation of Griseofulvin Binary and Ternary Solid Dispersions with HPMCAS. *AAPS PharmSciTech* **2009**, *10* (4), 1172–1177.
- (31) Prud'Homme, R. E. Miscibility phenomena in polyester/chlorinated polymer blends. *Polym. Eng. Sci.* **1982**, *22* (2), 90–95.
- (32) Ritger, P. L.; Peppas, N. A. A simple equation for description of solute release II. Fickian and anomalous release from swellable devices. *J. Controlled Release* **1987**, *5*, 37–42.
- (33) Aghdam, R. M.; Najarian, S.; Shakhesi, S.; Khanlari, S.; Shaabani, K.; Sharifi, S. Investigating the effect of PGA on physical and mechanical properties of electrospun PCL/PGA blend nanofibers. *J. Appl. Polym. Sci.* **2012**, *124* (1), 123–131.
- (34) Xiang, T. X.; Anderson, B. D. Molecular dynamics simulation of amorphous indomethacin-poly(vinylpyrrolidone) glasses: solubility and hydrogen bonding interactions. *J. Pharm. Sci.* **2013**, *102* (3), 876–91.
- (35) Vasanthavada, M.; Tong, W.-Q.; Joshi, Y.; Kislioglu, M. S. Phase Behavior of Amorphous Molecular Dispersions II: Role of Hydrogen Bonding in Solid Solubility and Phase Separation Kinetics. *Pharm. Res.* **2005**, *22* (3), 440–448.